

# The Interaction of a Novel Drug with $\beta$ -secretase-1 and Acetylcholinesterase: A Computational Investigation from Both Dynamics and Thermodynamics Viewpoints

Roosta, Sara; Hashemianzadeh, Seyed Majid\*<sup>+</sup>

Molecular Simulation Research Laboratory, Department of Chemistry, Iran University of Science and Technology,  
P.O. Box16846-13114 Tehran, I. R. IRAN

Gharaghani, Sajjad; Karimi Jafari, Mohammad Hossein

Department of Bioinformatics, Institute of Biochemistry and Biophysics, University of Tehran, Tehran, I.R. IRAN

**ABSTRACT:** Inhibition of glycogen synthase kinase-3 (GSK-3),  $\beta$ -secretase 1 (BACE-1) and acetylcholinesterase (AChE) could block one of the initial pathological events of Alzheimer's disease (AD). Recently, a new class of drugs has been developed with significant potential for GSK-3 inhibition. In this research, to the discovery of the new ligand as the potential multi-target drug with effective anti-Alzheimer's action a detailed computational investigation has been carried out on the effect of one of the most important drugs of such class on BACE-1 and AChE enzymes. The results of the binding free energies ( $\Delta G_{\text{Bind}}$ ) showed that the binding of this drug to AChE (-67.77 kJ/mol) is thermodynamically more favorable than BACE-1 (-22.35 kJ/mol). Examination of dynamic properties such as the root mean square fluctuation (RMSF) and the propensity for the secondary structure demonstrated that due to the decrease in the  $\beta$ -sheet and  $\beta$ -bridge content as well as the increase in the random coil content of BACE-1 in the presence of the drug, this enzyme was completely more flexible than AChE. The free-energy landscape (FEL) based on the first and second motion modes (PC1 and PC2) indicated that the large concerted motions of BACE-1 found in the simulations were particularly more sensitive to this drug than AChE.

**KEYWORDS:** Molecular dynamics simulation; Alzheimer's disease; Motion modes; Binding free energy; Free-energy landscape.

## INTRODUCTION

The most common type of dementia among the elderly is Alzheimer's Disease (AD), a chronic, progressive, and neurodegenerative disorder of the brain that involves deficiencies in cognitive functions, particularly mental

functioning. AD is responsible for dementia in more than 50 million people worldwide and will probably affect around 115 million people by 2050 [1].

Histologically, AD could be distinguished by the presence

---

\* To whom correspondence should be addressed.

+ E-mail: hashemianzadeh@iust.ac.ir

1021-9986/2023/5/1448-1463

16\$/6.06

of extracellular amyloid plaques and intraneuronal neurofibrillary tangles within the brain. The amyloid plaques are mainly made by an amyloid- $\beta$  ( $A\beta$ ) peptide, neurofibrillary tangles consist of aggregates of hyperphosphorylated  $\tau$  protein [2,3]. Currently, the treatment available for this disease is only symptomatic and mainly trying to counterbalance the neurotransmitter disorders associated with the disease [4].

The main therapeutic approaches associated with AD are the inhibition of some targets including  $\beta$ -site APP cleaving enzyme-1 (BACE-1), acetylcholine esterase (AChE), glycogen synthase kinase-3 beta (GSK-3) [5,6]. Among these, BACE-1 play a role in the rate-limiting step of the cleavage of the amyloid precursor protein (APP) contributes to the generation of the neurotoxic  $A\beta$  protein after the  $\gamma$ -secretase completes its function, and causes the development of AD [7]. AChE is a serine hydrolase whose main biological function is to terminate impulse transmission at cholinergic synapses by the rapid hydrolysis of the neurotransmitter acetylcholine (ACh) [8].

Role of  $\beta$ -secretase in Alzheimer's disease and amyloidogenic and non-amyloidogenic pathways well define. In non-amyloidogenic pathway, cleavage of amyloid precursor protein (APP) sequentially by  $\alpha$ - and  $\gamma$ -secretase produces soluble amyloid precursor protein alpha ( $sAPP\alpha$ ) and soluble P3, respectively. On the other hand, in amyloidogenic pathway,  $\beta$ - and  $\gamma$ -secretase produces  $sAPP\beta$  and insoluble  $A\beta$  protein, respectively, leading to the formation of  $\beta$  amyloid plaques [9,10].

AD is a multifactorial syndrome arising from multiple molecular abnormalities and it has been proven that a classic drug-design strategy based on the "one-molecule one-target" paradigm is clinically ineffective in the case of multifactorial diseases such as AD [11,12]. Therefore, in effective therapies, several drugs would have to be linked to multiple pathogenic targets. These types of drugs may be produced as part of a multiple treatment or a multiple-compounded drug. However, these methods could be detrimental to patients due to compliance issues, drug-drug interaction, bioavailability challenges and metabolism [13].

Due to the higher complexity for the prediction of pharmacodynamic and pharmacokinetic relationships in a single agent with respect to that of two or more, solving these issues is difficult [14,15]. Nowadays, the Multi-Target-Directed Ligands (MTDLs) method is a modern strategy that has brought new hope to this field [16].

The assumption that makes this strategy is based on the ability of a compound to hit multiple targets [17,18].

Such MTDLs are expected to have a better therapeutic profile to combat such complex diseases [19,20]. In recent years, a number of promising MTDLs have been proposed for the treatment of AD [5]. In order to design new compounds with multi-target characteristics, *in silico* drug designing or computer-aided drug discovery (CADD) has been made colossal progress in the development of drugs such as small organic molecules, aptamers, peptides, and antibodies [21].

CADD is a cost-effective technique that significantly affects the drug development process by reducing the total time from identifying a target to hitting discovery and optimization [22]. The main advantage of CADD is the ability to generate a large number of compounds and screen them for a target-specific binding [23].

Lately, many of these techniques have been the key tools in Multi-Target Drug Discovery (MTDD) to identify drugs that interact simultaneously with multiple target agents. These techniques are considered into combinatorial and fragment-based approaches. Conventionally, to find virtual hits for each target, combinatorial approaches conduct parallel searches to specify which hit has an interaction with more than a target [24].

Due to such inquiries, new drugs for targets have been discovered in order to be used for a disease and/or to decrease resistance. The major consideration in drug discovery has been attracted to the design and development of a single chemical that acts simultaneously at multiple molecular targets [25]. New small molecules as an inhibitor have recently been created for a wide range of biological targets, as considerable signs of progress have been obtained in computational drug design methods, including Molecular Dynamics (MD) simulations and virtual screening (VS), as well as increased access to large chemical repositories and the availability of crystallographic data [26].

Molecular dynamics simulations are powerful tools for understanding the atomic-detailed mechanism behind the interactions of protein-ligand, protein-protein, peptides, bio-membranes, and  $A\beta$ - organic salts [27–31], which greatly contribute to revealing limitations and shed light on the design of new drugs [32]. The MD simulation results could be used to expound structure–affinity relationships. Those pieces of information derived can

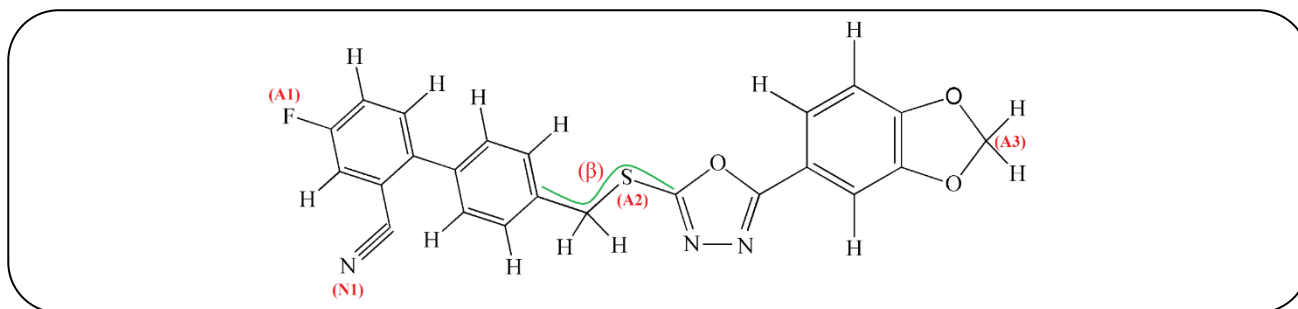


Fig. 1: Molecular structure of ligand.

increase our comprehension of the crucial interactions at the active-sites of the targets and the data can be applied to discovery as well as design better Multi-Target-Directed Ligands (MTDLs) [33–35].

## THEORETICAL SECTION

### Virtual screening

At first, the results of virtual screening for BACE-1 [36] and AChE [37] were compared among themselves to search for compounds included in the top best compounds for each target from the ChEMBL [38,39] and BindingDB [40] database with IC<sub>50</sub> of < 5 nM for each protein as the target, for which around 400 compounds were selected with smallest IC<sub>50</sub>. After selecting the inhibitors for these targets, the virtual screening of drugs against the structure of target proteins was performed individually using AutoDock Vina in PyRx 8.0 virtual screening tool [33]. The top three drugs with the highest binding energy scores against each protein were selected as Alzheimer's disease treatment compounds for further assessment. Among those, a novel scorpion-shaped GSK-3 inhibitor (14b) [41], from now on being called *ligand*, was selected to examine its effect on AChE and BACE-1 proteins as shown in Fig. 1.

Crystal structures for all the targets were obtained from the Protein Data Bank (BACE-1, PDB code: 6EQM; AChE, PDB code: 4M0E). The modifications to the PDB files of the proteins were done before the docking process. Water molecules and other cofactors were omitted as well as the co-crystallized ligand. All the missing residues in the structures were monitored and fixed with the aid of a loop modeling server. Multiple bond orders based on correct definitions were then checked; using the REDUCE software program all hydrogen atoms were added [42].

### Molecular docking

The docking was conducted by AutoDock4.2 [43] for ligand and the targets. The AutoDock package involves AutoGrid and AutoDock programs. The calculation of energy grid maps are done through which the AutoGrid program. Here, a  $60 \times 60 \times 60$  point's grid size with a spacing of  $0.375 \text{ \AA}$  was determined. The conformation search and energy evaluation is done by AutoDock program; during the docking experiments the following parameters were applied: crossover rate (0.8), number of GA runs (300), mutation rate (0.02), and population size (150). Grid spacing and other parameters were applied as default values. With a maximum of 270000 generations, docking simulations were conducted for up to 2.5 million energy evaluation steps. In AutoDock, a set of 300 docked conformations was produced using the docking simulation. The best binding conformations between ligands and the protein were taken based on the lowest-energy conformations generated by AutoDock.

### Molecular dynamics simulation details

In this study, four different simulation systems were set up to study the behaviour of the ligand-proteins (Fig. 1) in the presence and absence of AChE and BACE-1 proteins. All simulations were carried out in the NPT ensemble and by GROMACS 5.1.5 package [44–46]. For both ligand and proteins the CHARMM27 force field were used [47,48]. The temperature maintained at 300 K and controlled by the Nose-Hoover thermostat with a coupling time of 0.5 ps [49]. Parrinello-Rahman barostat, with a coupling time constant of 2 ps was used to hold constant at 1 bar [50]. The bond lengths were constraint using the LINCS algorithm [51]. The leap-frog algorithm with a time step of 2 fs was used to integrate the Newton's equations of motion [52]. A 1.2 nm distance were set as a cut-off for both Coulomb and van der Waals (vdW)

interactions, and the long-range Coulomb interaction was considered through the particle mesh Ewald (PME) method [53]. All of the systems were hydrated by the transferable intermolecular potential 3 point (TIP3P) water model [54] and with periodic boundary conditions in all three dimensions. In all systems, steepest descent energy minimization was applied to remove unfavorable atomic contacts and calm down the water molecules within the systems [55]. At first, equilibrations in the NVT ensemble for 1 ns and then in NPT ensemble for 9 ns were conducted by restraining the positions of ligand and proteins. After that, simulations were carried out for 50 ns as a final simulation step without any restrictions. By using of VMD visualizations of systems were created [56]. To estimate the receptor-ligand affinity energy was calculated by Molecular Mechanics-Poisson Boltzmann Surface Area (MM-PBSA) method [57,58]. The binding energy was estimated according to the following equation:

$$\Delta G_{\text{binding}} = \Delta G_{\text{complex}} - \Delta G_{\text{protein}} - \Delta G_{\text{ligand}} \quad (1)$$

Where  $\Delta G_{\text{complex}}$  shows the total free energy of the protein-ligand complex,  $\Delta G_{\text{protein}}$  and  $\Delta G_{\text{ligand}}$  express the free energy of protein and ligand individually in the solvent, respectively.

For each term in Eq.1, the free energy could be expressed as:

$$G = E_{\text{MM}} - G_{\text{sol}} - TS \quad (2)$$

Which  $E_{\text{MM}}$  is the average molecular mechanical potential energy in a vacuum [59] that includes electrostatic ( $E_{\text{elec}}$ ) and van der Waals ( $E_{\text{vdw}}$ ) interactions.  $G_{\text{sol}}$  represents the free energy upon solvation.  $TS$  term is the entropy contribution to the free energy, where  $T$  and  $S$  are temperature and entropy, respectively.

## RESULTS AND DISCUSSION

### Stability of structures and binding of ligand to proteins

The stability of the protein relative to its conformation can be determined by the deviations that occur in its simulation. Therefore, by monitoring of the root mean square deviation (RMSD) of backbone considering its starting structures was examined, Fig. 2.

Protein RMSD values in the BACE-1 containing systems show an increase early in the simulation. Then the equilibration was obtained in both systems after 6 ns,

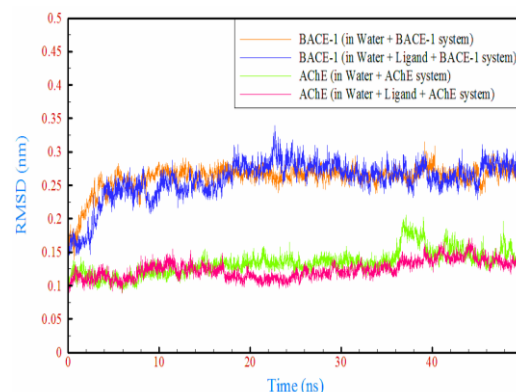


Fig. 2: Root mean square deviation (RMSD) of enzymes in different simulated system.

so that the RMSDs fluctuated around 0.27 nm, and a flat region until the end of the simulations was continued. For BACE-1, in the ligand-containing system, the fluctuations around the equilibrium value are more obvious up to the middle of the simulation time (25 ns). In the case of AChE systems, a flat area is seen from the beginning of the simulation, indicating that these systems have been equilibrated. After ensuring equilibrium, the binding site for each system was carefully considered. One of the common measurements for considering affinity in a protein-ligand system is the distance between the binding site of a protein with the ligand [60,61]. In this study, by defining a distance of 0.3 nm between all residues and the ligand's Center of Mass (COM) in at last 5ns, as summarized in Table 1, the binding sites were revealed.

To clarify more, the situation of the ligand relative to the residues of the binding site at the beginning (initial structure obtained from docking calculations) and the end of the simulation (final structure obtained from 50 ns molecular dynamics) is shown in Fig. S1. As can be seen, the ligand entered the active site of the AChE on the fluorine side, while in the BACE-1 it occurred on the opposite side of the fluorine. This difference in ligand loading within the cavities of proteins as well as the nature of the active-site inspired subsequent thermodynamic and dynamic studies.

## THERMODYNAMICS PROPERTIES

### Hydrogen bond

Analysis of receptor-ligand interactions in different ligand-protein systems indicated that among the non-bonded interactions, the hydrogen bonds are critical

**Table 1: Distances between protein residues and Ligand.**

Ligand in BACE-1 containing system		
Residue number	Residue type	Average distance of glutathione (nm)
1	PHE49	0.285 ( $\pm 0.020$ )
2	THR74	0.232 ( $\pm 0.020$ )
3	GLN75	0.256 ( $\pm 0.010$ )
4	LYS109	0.248 ( $\pm 0.050$ )
5	ILE112	0.234 ( $\pm 0.040$ )
6	ASN113	0.224 ( $\pm 0.020$ )
Ligand in AChE containing system		
1	PHE533	0.278 ( $\pm 0.020$ )
2	TRP530	0.269 ( $\pm 0.020$ )
3	PHE529	0.276 ( $\pm 0.020$ )
4	ALA526	0.300 ( $\pm 0.040$ )
5	LEU371	0.250 ( $\pm 0.030$ )
6	ALA372	0.246 ( $\pm 0.023$ )
7	ALA375	0.256 ( $\pm 0.020$ )
8	LEU378	0.287 ( $\pm 0.050$ )
9	HIS379	0.251 ( $\pm 0.025$ )
10	TYR380	0.267 ( $\pm 0.030$ )

determinants for ligand binding affinity [62,63]. Hence, in order to evaluate the residues responsible for ligand binding, intermolecular hydrogen bonds for protein-ligand complexes were investigated. In the BACE-1 containing system, it was found that only ASN113 and GLN75 residues were able to make 0.86 and 0.03 hydrogen bonds with the ligand, respectively, and the other residues did not show any bond with the ligand. However, in the AChE containing system, no hydrogen bonding was found between the ligand and the active-site residues. These results indicate that the hydrogen bonds between the ligand and the active-site residues did not affect the loading of the ligand. An important result in this section is the difference in the hydrogen bond between water and the ligand, due to the difference in the dipole moment of the ligand in the two simulated systems. So that, in AChE and BACE-1 containing systems the ligand was able to make 3.2 and 2.6 hydrogen bonds with the water molecules and the ligand dipoles were 4.2 and 3.9 (Debye), respectively. As seen, more dipole moment caused an increase in the hydrogen

bond between the ligand/water in the AChE containing system. Another reason for this observation can be related to the preferential orientation of the ligand on the active-site, so that the opposite side of the fluorine, which has more oxygen atoms, is accessible to water (Fig. S1) and facilitated hydrogen bonding with water.

### Binding free energies and interaction analysis

To estimate binding free energies ( $\Delta G_{\text{bind}}$ ) and relative stability of the ligand in the BACE-1 and AChE, the MMPBSA method was applied and are summarized in Table 2.

The binding free energy ligand/BACE-1 is much stronger than in ligand/AChE, and in both systems, the van der Waals (vdW) contribution is a vital determinant, and the electrostatic contribution is much lower. For more detailed insights, ligand interaction energies with the active-site residues were examined, Table 3. Since the ligand has multiple aromatic rings and also contains two oxygen on the opposite fluoride side, having both hydrophilic and hydrophobic parts in its structure. In the ligand/BACE-1 system, the residues of ILE112 and PHE49 are both hydrophobic and the ligand was inserted into the BACE-1 cavity via its hydrophilic side (oxygen-containing side). Consequently, the hydrophobic aromatic rings of the ligand were also placed close to the ILE112 and PHE49 residues (Fig. S1a), which resulted in favourable vdW interactions -16.56 and -10.84 kJ/mol, respectively. In the ligand, as shown in Fig.1, the most negative charge is related to the nitrogen atom N1 (-0.557), so due to N1 containing ring being located near ASN113, a very favorable electrostatic interaction (-10.65 kJ/mol) occurs with the polar amino acid ASN113. GLN75 and THR74 are polar neutral side chain amino acids, so predominant interactions between nitrogen and oxygen atoms of the oxadiazole ring of the ligand with these residues are vdW type. In the ligand/AChE system, since the loading is done from the hydrophobic side of the ligand (fluorinated part), almost all residues that interact with the ligand, including ALA, PHE, TYR, TRP, and LEU, are hydrophobic. Meanwhile, over half of the total interaction energy ( $\sim -75$  kJ/mol) is associated with ALA and PHE residues. A protein's (or ligand's) function depends not only on its thermodynamics, but also on its structural changes. A ligand can alter the function of a protein by interfering with the essential motions of a protein as well

**Table 1: Comparison of the binding free energy and various energy components.**

Systems	Energy components (kJ/mol)	$\Delta E_{elec}$	$\Delta E_{vdw}$	$\Delta G_{polar}$	$\Delta G_{nonpolar}$	$\Delta G_{bind}$
Water + Ligand + BACE-1		-4.86 ( $\pm 0.13$ )	-37.89 ( $\pm 0.89$ )	24.86 ( $\pm 1.02$ )	-4.46 ( $\pm 0.10$ )	-22.35 ( $\pm 0.92$ )
Water + Ligand + AChE		-10.29 ( $\pm 0.13$ )	-109.29 ( $\pm 0.58$ )	63.93 ( $\pm 0.47$ )	-12.12 ( $\pm 0.06$ )	-67.77 ( $\pm 0.67$ )

**Table 2. Analysis of interaction energies (kJ/mol) between the active-site residues and ligand.**

Ligand in BACE-1 containing system		
Different components Proteins residues	Ligand (Columbic)	Ligand (vdW)
PHE49	-0.72 ( $\pm 0.35$ )	-10.84 ( $\pm 2.60$ )
THR74	0.03 ( $\pm 0.04$ )	-1.29 ( $\pm 0.64$ )
GLN75	1.05 ( $\pm 0.14$ )	-10.62 ( $\pm 1.20$ )
LYS109	-3.54 ( $\pm 1.80$ )	-16.08 ( $\pm 1.20$ )
ILE112	-7.61 ( $\pm 1.70$ )	-16.56 ( $\pm 1.40$ )
ASN113	-10.65 ( $\pm 2.80$ )	-2.30 ( $\pm 0.78$ )
Sum	-21.44	-57.69
Ligand in AChE containing system		
PHE533	-0.28 ( $\pm 0.26$ )	-20.01 ( $\pm 0.64$ )
TRP530	-6.45 ( $\pm 0.11$ )	-17.95 ( $\pm 0.40$ )
PHE529	2.83 ( $\pm 0.07$ )	-18.35 ( $\pm 0.30$ )
ALA526	-1.53 ( $\pm 0.07$ )	-4.10 ( $\pm 0.15$ )
LEU371	-3.29 ( $\pm 0.40$ )	-15.86 ( $\pm 0.13$ )
ALA372	-0.23 ( $\pm 0.03$ )	-13.12 ( $\pm 0.17$ )
ALA375	-1.28 ( $\pm 0.11$ )	-19.16 ( $\pm 0.17$ )
LEU378	0.15 ( $\pm 0.02$ )	-6.29 ( $\pm 0.15$ )
HIS379	-2.40 ( $\pm 0.26$ )	-6.82 ( $\pm 0.13$ )
TYR380	-0.14 ( $\pm 0.08$ )	-3.08 ( $\pm 0.05$ )
Sum	-12.62	-124.74

as the interactions of the active-site. In particular, the essential motions induced by the conformational changes [64]. Deviations in the structure of the ligand and proteins in the simulated systems were examined separately in two sections, which are discussed in detail as follows.

### DYNAMIC PROPERTIES AND STRUCTURAL DEVIATIONS OF LIGAND

To investigate the dynamic properties of the influence of proteins on the ligand, the Mean Square Displacement (MSD)

of the ligand in both protein-containing systems was considered, Fig. 3. As can be seen, the ligand movement in the AChE system is far lower than BACE-1. According to Table 3, the interaction energies of the ligand with the active-site residues in the AChE system are almost two times more than the BACE-1, and the number of residues around the ligand is more than the active-site residues in the BACE-1 system. Therefore, the possibility of movement has been severely limited. Another reason, which is less important, is the more hydrogen bonds that the ligand is made with water. Altogether, stronger interactions with the active-site and more hydrogen bonding with water appear to thermodynamically limit the ligand on both sides and the lack of space due to the more residues in the active-site dynamically reduces the movement in AChE containing system. To determination of compactness level in the structure and solvent accessibility of ligand in both systems, radius of gyration (Rg) and solvent accessible surface area (SASA) analysis were done, Table S1. Analysis of radius of gyration provides us an insight of the overall dimensions of the protein and ligand. However, the simultaneous study of Rg and SASA shows that the ligand compactness was not significantly different in both systems. The ligand RMSD values in the two systems are greater than 0.3 nm, indicating that the ligand was flexible when interacting with the two proteins. To get a precise insight of the ligand structure, an angle ( $\alpha$ ) between the three atoms (specified as A1, A2, and A3 in Fig. 1) as well as a dihedral angle ( $\beta$ ), were assigned to the ligand for measuring structural changes.

Simultaneous examination of these angles can be advantageous because the internal coordinates naturally provide a correct separation of internal and overall motion. Fig. S2a shows the ( $\alpha$ ) distribution obtained from the simulation, which prognosticates that mainly two conformational states are populated in the AChE containing system. One of them occurred between  $\sim 75$ - $90^\circ$  and another one is a region between  $\sim 165$ - $175^\circ$ . However, only one state was seen in the BACE-1 containing system between  $\sim 150$ - $155^\circ$ . Angular distribution of  $\beta$  in the AChE containing system, shown in Fig. S2b, revealed that the

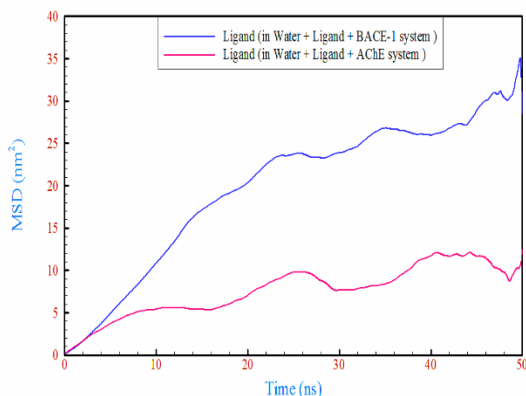


**Fig. 3:** The mean square displacement (MSD) of ligand in different simulated system.

structures were populated with  $\beta=90^\circ$  as the same (even greater than) at  $\beta=180^\circ$ . Finally, it is observed that the value of the  $\beta$  angle in the BACE-1 containing system was often around  $180^\circ$ , although structures with  $\beta=90^\circ$  also occurred. Given the angular distributions, more information about the flexibility and predominant configuration of the ligand interaction with BACE-1 and AChE can be obtained from the free-energy landscape, as shown in Fig. 4. A free energy landscape may be characterized by its minima that represent metastable conformational states and its barriers that connect these states. It can be seen that the ligand in the BACE-1 containing system gets trapped in many local minima in the range of  $\alpha=60-175^\circ$  and  $\beta=50-180^\circ$ , which seems to be faced with less energy barrier to converting from one configuration with certain angles to another configuration. However, the ligand in the AChE containing system can be taken more limited  $\alpha$  and  $\beta$  angles ( $\alpha=60-120^\circ$  and  $\beta=50-100^\circ$  as well as  $\alpha=120-180^\circ$  and  $\beta=140-180^\circ$ ), so that it showed more specific local minima. Representative structures are identified and clearly depicted in Fig. 4. As a result, the ligand had taken a more flexible structure in BACE-1 and shown diverse configurations with lower surface energy, while in AChE it adopted a rigid structure with more specific angles.

## DYNAMICS PROPERTIES AND STRUCTURAL DEVIATIONS OF PROTEINS

### Root Mean Square Fluctuation (RMSF)

The dynamic behavior of individual amino acid residues for proteins was determined in terms of RMSF values. This analysis is useful for describing local

differences in flexibility between residues throughout MD simulation [65]. As shown in Fig. 5, compared to the ligand-free system, BACE-1 shows an overall higher degree of flexibility in the ligand-containing system, and significant changes are seen.

So that, the average RMSF values in the lig/BACE-1 and BACE-1 systems were 0.124 and 0.082 nm, respectively. The difference in the flexibility of the active-site residues (Table S2) shows that the most change was related to PHE49, LYS109, ILE112, and ASN113 while GLN75 did not change and THR74 showed a decrease. In both systems, the most fluctuations were related to the 303-311 residues, which could be because more than half residues (GLU302, ASP303, ASP309, ASP310) were electrically charged (negatively charged), and the electrostatic repulsion between these residues has been increased the flexibility. However, AChE showed low fluctuations, Fig. 5b. As can be seen, the flexibility of AChE residues in the ligand-free system is not significantly different from that of the ligand-containing system, and the average RMSF values were 0.081 and 0.080, respectively. A similar observation is found regarding the flexibility of the active-site residues of AChE (Table S2). The results indicate that two regions of the AChE structure have significant fluctuations. One contains 76-85 residues (TYR75, PRO76, GLY77, PHE78, GLU79, GLY80, THR81, GLU82, MET83, and TRP84) which are mostly hydrophobic. Another among the residues 259-263 (GLY258, GLY259, THR260, GLY261, and GLY262) in which GLY is as the simplest and lightest amino acid.

### Analyses of secondary structures

Protein structure is inherently important because the structure of a protein is directly related to its function. The propensity of the secondary structural content is an essential element to study the structural behavior of the protein [66]. Changes in the secondary structure were examined in BACE-1 and AChE, as shown in Figures 6 and 7. The secondary structure results of BACE-1 show that in the ligand-containing system, the Coil content is more than the ligand-free system, while the Bend content remains almost constant. In addition, the  $\beta$ -sheet and  $\beta$ -bridge content clearly decreased, especially at the end of the simulation time. And finally is seen the  $\alpha$ -Helix, Turn, and 3-Helix content remain constant. Therefore,

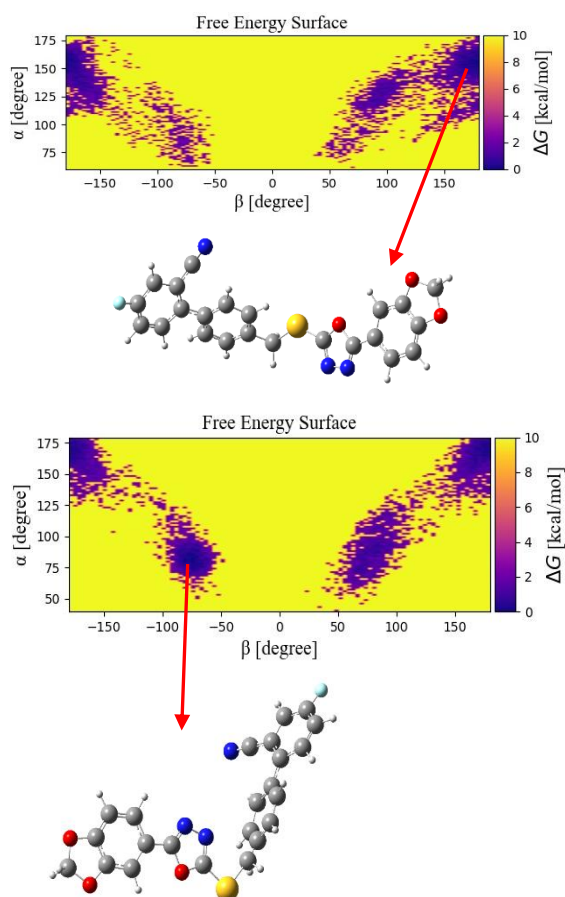


**Fig. 4:** 2D representations of the free-energy landscape of ligand in BACE-1 (a), AChE containing system (b).

It is suggested that increasing the coil as well as decreasing  $\beta$ -leaf and  $\beta$ -bridge greatly increases the fluctuation of BACE-1 in the ligand-containing system. Residues that are predominantly  $\beta$ -sheet are indicated in the RMSF by the green line (C1, C2, and C3 in Fig. 5a and S3). It can be seen that these residues in both BACE-1 containing systems, have relatively less flexibility than other residues. It is well known, the hydrogen bonding which occurs between the carboxyl oxygen and the amine hydrogen of the backbone of a protein is the main driving force behind the secondary structure [67]. Examination of hydrogen bonds (Table S3) showed that in the ligand-containing system, the number of parallel and anti-parallel bridges hydrogen bonds within BACE-1 structure is drastically reduced than the ligand-free system, which in turn can be considered as a reason to decreasing the propensity of  $\beta$ -sheet and  $\beta$ -bridge and increasing fluctuations. The results of the AChE secondary structure show that in the

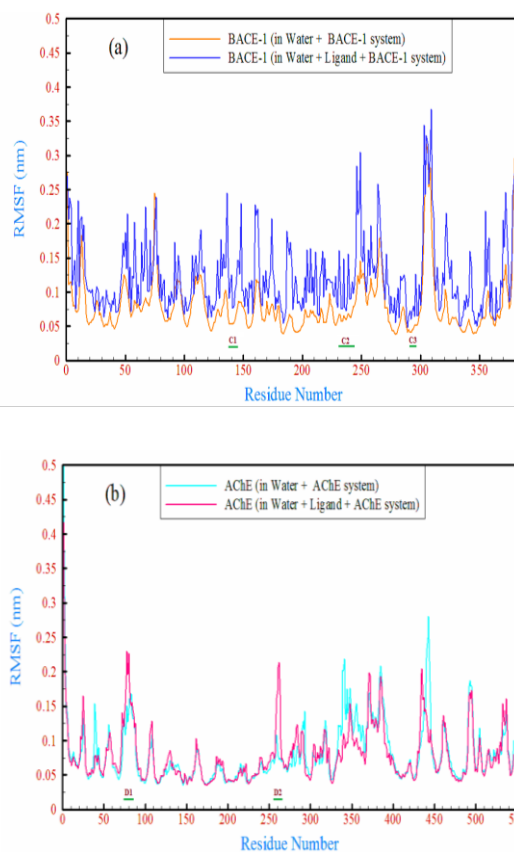


**Fig. 5:** Root mean square fluctuation (RMSF) of BACE-1 (a), and AChE (b) in different simulated system.

ligand-containing system, the Coil content is slightly increased compared with the ligand-free system, but the Bend content is also reduced. Another contrary propensity is to reduce the  $\beta$ -sheet content, while  $\alpha$ -Helix is increased. Overall, there was no significant difference in the fluctuations of AChE containing systems, so flexibility has changed locally. One can see that in the ligand-containing system, residues 75-85 have been changed to the Coil and Bend content (D1 in Fig. 5b and S2). Therefore, an increase in fluctuations occurs in this region. Also, residues 255-265 have been changed to the Bend to some extent (D2 in Fig. S4), therefore the fluctuations of these residues have increased, as shown in Fig. 5. Another important finding in this regard is the lack of significant change in the number of parallel and anti-parallel bridges hydrogen bonds within the AChE structure (Table S3), which can be considered a reason for the low fluctuations observed in the ligand-containing system.

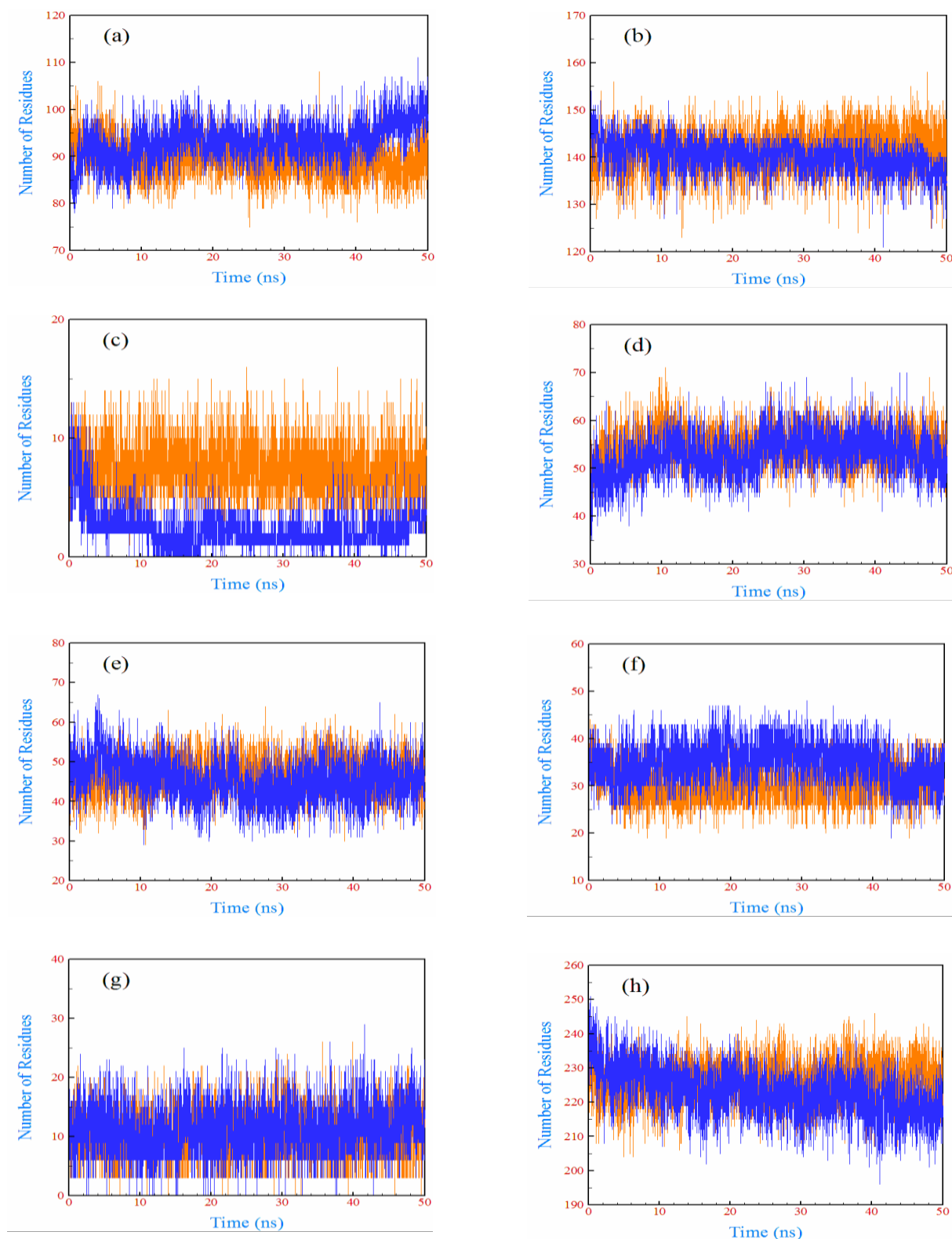


**Fig. 6:** Secondary structure changes of BACE-1 during the course of 100-ns MD simulation Coil (a), B-Sheet (b), B-Bridge (c), Bend (d), Turn (e), A-Helix (f), 3-Helix (g), Structure (h) in ligand-free system (orange) and ligand-containing system (blue).

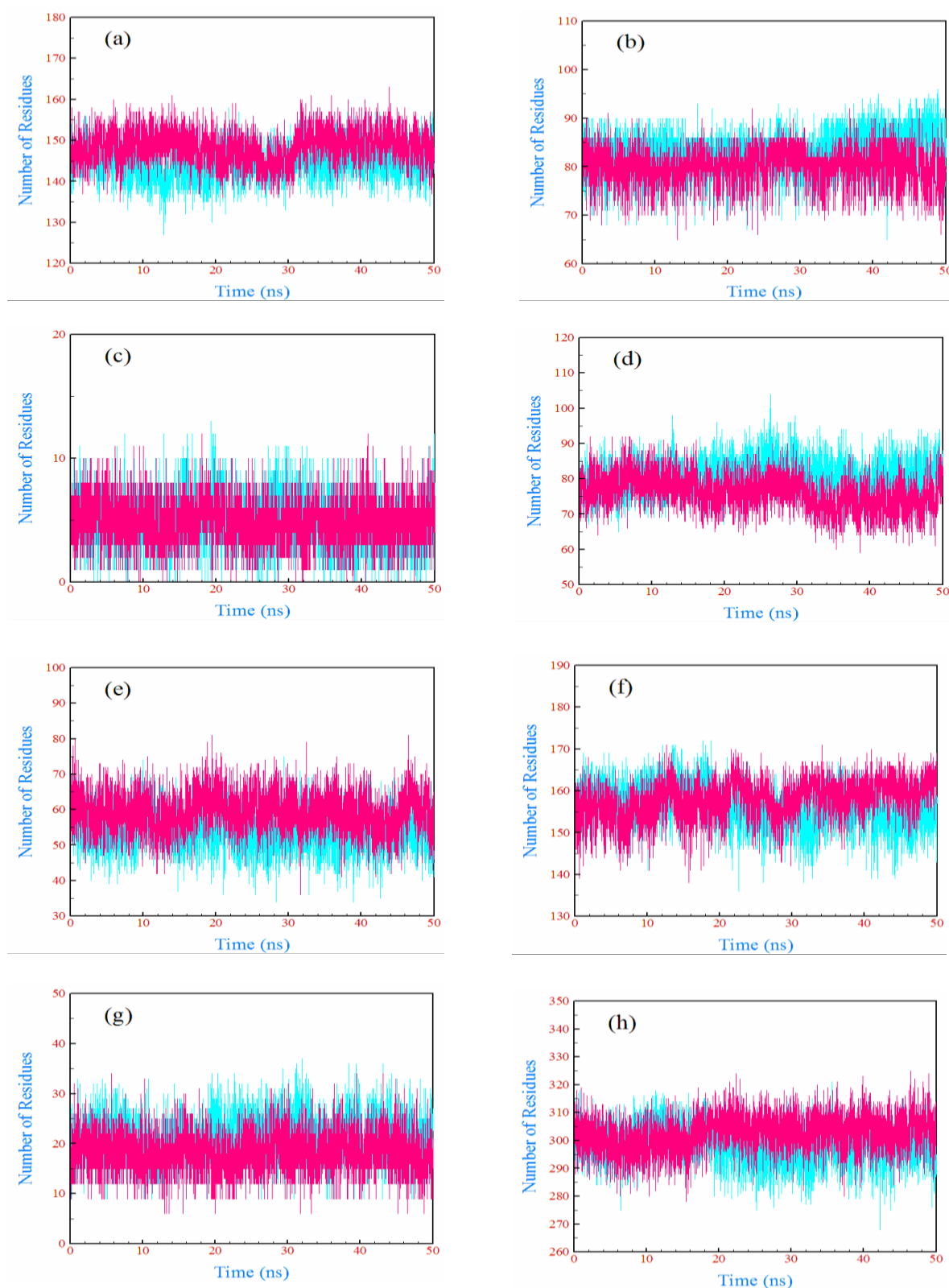


**Fig.7:** Secondary structure changes of AChE during the course of 100-ns MD simulation Coil (a), B-Sheet (b), B-Bridge (c), Bend (d), Turn (e), A-Helix (f), 3-Helix (g), Structure (h) in ligand-free system (cyan) and ligand-containing system (pink).

### Ramachandran plot analysis

The Ramachandran plot is the 2D plot of the  $\phi$ - $\psi$  torsion angles that played a central role in understanding the protein structure. Each range of  $\phi$ - $\psi$  values in the Ramachandran plot relates to a particular secondary structure and shows the possible conformations of  $\phi$  and  $\psi$  angles for a protein. The conformations in which the atoms in the protein come closer than the sum of their Vander Waals radii and demonstrated by the white (disallowed for all amino acids except glycine). The partially allowed regions of the left-handed helix where the atoms are allowed to come a little closer together and shown by the yellow. Red regions are related to the  $\alpha$ -helical and  $\beta$ -sheet conformations, wherein there are no steric clashes (allowed regions) [68]. In this study, the Ramachandran plot was evaluated to examine the active-site residues and their structural changes. The analyses of the Ramachandran plots produced by PROCHECK [69,70] are given in Fig. S5. The results indicated that most of the residues were in the favorable areas (more than 90%). The Ramachandran plot was divided into two areas for detailed analysis of the conformations. Residues having torsion angles in the range  $-135 < \phi < -38^\circ$ ,  $-72 < \psi < 27^\circ$  were considered to be in the  $\alpha$ -helical region. Residues having torsion angles in the range  $-171 < \phi < -38^\circ$ ,  $90 < \psi < 180^\circ$  were considered to be in the  $\beta$ -sheet region. Then, the active-site residues were carefully studied (Table S4). In the case of BACE-1, three residues (PHE49, THR74, and LYS109) in the ligand-free system were changed from  $\alpha$ -helical to  $\beta$ -sheet structure in the ligand-containing system, and the  $\beta$ -sheet structure was seen for GLN75, ILE112, and ASN113 in both systems. However, a different finding was obtained for AChE, so that all of the active-site residues remained within the  $\alpha$ -helical region in both systems and just small changes were seen.

### Principal Component Analysis (PCA)

By reducing the number of dimensions of the data obtained from molecular dynamics simulations, one can be identifying the dynamical behavior of proteins by projecting the trajectory on small dimensions in terms of principal components (PCs) [67]. Hence, by taking the trajectory of the molecular dynamics simulations, the dominant modes in the motion of BACE-1 and AChE in the different simulated systems were extracted, as shown in Fig. 8. If the motions are similar, the eigenvectors and

eigenvalues from the individual trajectories must be similar. Principal components analysis (PCA) was carried out on the backbone atoms in BACE-1 and AChE proteins. Such analysis showed that the first two eigenvectors account for  $> 40\%$  of all the motion in BACE-1 and AChE (Fig. S6). The protein concerted motions are identified by the first few eigenvalues and decrease rapidly in amplitude to reach some more localized and constrained fluctuations. Fig. 8a shows that the properties of the motions described by the first few PCs differ for the ligand-containing and ligand-free systems in both proteins. To find the most stable configurations for each protein and qualitative inspection to find that what the energy barriers are between different conformational basins, the free energy counter maps constructed for all systems, as shown in Fig. 8b. It was found that the PC1 and PC2 motion modes of BACE-1 in ligand-containing system spanned larger ranges than that ligand-free system, indicating conformational rearrangements caused by the ligand. More red spots in the free-energy landscape BACE-1 in the ligand-containing system show that more motion modes, without significant barrier, are accessible and this is in agreement with those findings of reducing the intramolecular hydrogen bonds (Table S3) and increasing the RMSF (Fig. 5a). To identify the main local deviations, the first modes of motion in both systems were taken into account simultaneously. As can be seen in Fig. S7, the most of the deviations are related to a  $\beta$ -hairpin region (C), an  $\alpha$ -helix region (D), and finally some other different coils (A and B). However, in the case of AChE, the distinctive local basins were observed, although these minima were more localized in the ligand-containing system with fewer red and orange spots.

### CONCLUSIONS

A computational study of the protein-ligand complex based on the dynamics and thermodynamics effects of a well-known drug on the two amyloid-beta-precursor proteins (BACE-1 and AChE enzymes) was done. According to the MSD results, due to the stronger interaction energies between drug/active-site residues, the movement of the drug in the AChE-containing system was less than that of BACE-1. The drug showed different mechanisms of binding in the active-site of proteins, and therefore, the drug tended to be bound to the active-site of BACE-1 from the opposite side of fluorine, while it was

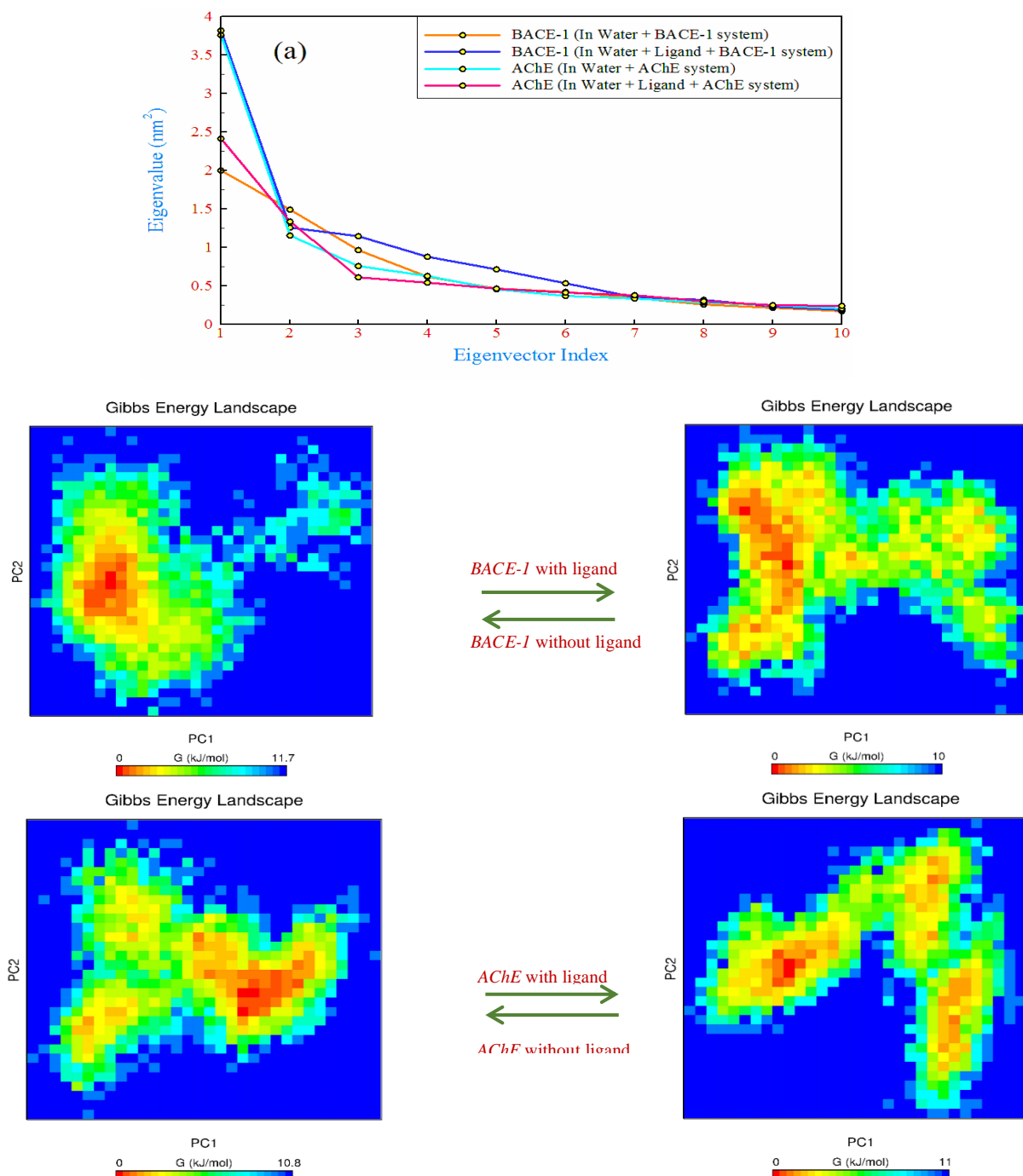


**Fig. 8:** Eigenvalue versus eigenvector index of proteins (a), free-energy landscape between PC1 and PC2 of BACE-1 and AChE in different simulated systems (b).

bound to the active-site of AChE from the fluorine side. The free-energy landscape (FEL) based on the internal angles ( $\alpha$  and  $\beta$ ) showed that the drug was more flexible in the BACE-1-containing system than that of AChE. Analyzing the RMSF revealed that in the presence of the drug, BACE-1 was affected more than AChE and had great

flexibility, it was especially noticeable when comparing active-site residues in two systems. The results obtained from the secondary structural content in the BACE-1 containing systems demonstrated a decrease in the propensity of  $\beta$ -sheet and  $\beta$ -bridge in the presence of the drug, which in turn could be due to the reduction in the number

of parallel and anti-parallel bridges hydrogen bonds within BACE-1 structure. The results of ligand/active-site residues study showed that the hydrogen bonding was ineffective in ligand binding to both enzymes, and van der Waals (vdW) interactions play a decisive and dominant role. Compared to the ligand-free system, the active-site residues of BACE-1 in the ligand-containing system tended to adopt the  $\beta$ -sheet structure, whereas the active-site residues of AChE remained  $\alpha$ -helical in both simulated systems. Investigation of the active-site residues of BACE-1 showed that PHE49, THR74, and LYS109 in the ligand-free system were changed from  $\alpha$ -helical to  $\beta$ -sheet structure in presence of the drug, while in both systems containing/free of drug, all of the active-site residues of AChE remained within the  $\alpha$ -helical region. By considering the principal component analysis (PCA) it was found that due to the presence of drug, conformational rearrangements occurred in BACE-1 and the PC1 and PC2 motion modes spanned larger ranges compare to the ligand-free system.

Received : May 19, 2022 ; Accepted : Sep. 26, 2022

## REFERENCES

- [1] Rochais C., Lecoutey C., Gaven F., Giannoni P., Hamidouche K., Hedou D., Dubost E., Genest D., Yahiaoui S., Freret T., [Novel multitarget-directed ligands \(MTDLs\) with Acetylcholinesterase \(AChE\) Inhibitory And Serotonergic Subtype 4 Receptor \(5-HT4R\) Agonist Activities as Potential Agents Against Alzheimer's Disease: the Design of Donecopride](#), *J. Med. Chem.*, **58**: 3172–3187 (2015).
- [2] Gazova Z., Soukup O., Sepsova V., Siposova K., Drtinova L., Jost P., Spilovska K., Korabecny J., Nepovimova E., Fedunova D., [Multi-target-directed Therapeutic Potential of 7-Methoxytacrine-Adamantylamine Heterodimers in the Alzheimer's Disease Treatment](#), *Biochim. Biophys. Acta (BBA)-Molecular Basis Dis.*, **1863**: 607–619 (2017).
- [3] Maas T., Eidenmüller J., Brandt R., [Interaction of Tau with the Neural Membrane Cortex Is Regulated by Phosphorylation at Sites that Are Modified In Paired Helical Filaments](#), *J. Biol. Chem.*, **275**: 15733–15740 (2000).
- [4] Melnikova I., [Therapies for Alzheimer's Disease](#), *Nat. Rev. Drug Discov.*, **6**: 341–342 (2007).
- [5] Moussa-Pacha N.M., Abdin S.M., Omar H.A., Alniss H., Al-Tel T.H., [BACE1 Inhibitors: Current Status And Future Directions In Treating Alzheimer's Disease](#), *Med. Res. Rev.*, **40**: 339–384 (2020).
- [6] Pohanka M., [Inhibitors of Acetylcholinesterase And Butyrylcholinesterase Meet Immunity](#), *Int. J. Mol. Sci.*, **15**: 9809–9825 (2014).
- [7] Zagórska A., Jaromin A., [Perspectives for New and More Efficient Multifunctional Ligands for Alzheimer's Disease Therapy](#), *Molecules*, **25**: 3337 (2020).
- [8] Tougu V., [Acetylcholinesterase: Mechanism of Catalysis and Inhibition](#), *Curr. Med. Chem. Nerv. Syst. Agents.*, **1**: 155–170 (2001).
- [9] Mouchlis V.D., Melagraki G., Zacharia L.C., Afantitis A., [Computer-Aided Drug Design of B-Secretase,  \$\Gamma\$ -Secretase and Anti-Tau Inhibitors for the Discovery of Novel Alzheimer's Therapeutics](#), *Int. J. Mol. Sci.*, **21**: 703 (2020).
- [10] Ullah M., Johora F.T., Sarkar B., Araf Y., Ahmed N., Nahar A.N., Akter T., [Computer-Assisted Evaluation of Plant-Derived  \$\beta\$ -Secretase Inhibitors in Alzheimer's Disease](#), *Egypt. J. Med. Hum. Genet.*, **22**: 1–15 (2021).
- [11] Citron M., [Alzheimer's Disease: Strategies for Disease Modification](#), *Nat. Rev. Drug Discov.*, **9**: 387–398 (2010).
- [12] Rosini M., Simoni E., Minarini A., Melchiorre C., [Multi-Target Design Strategies in the Context of Alzheimer's Disease: Acetylcholinesterase Inhibition and NMDA Receptor Antagonism as the Driving Forces](#), *Neurochem. Res.*, **39**: 1914–1923 (2014).
- [13] Morphy R., Rankovic Z., [Designed Multiple Ligands. an Emerging Drug Discovery Paradigm](#), *J. Med. Chem.*, **48**: 6523–6543 (2005).
- [14] Kola I., Landis J., [Can the Pharmaceutical Industry Reduce Attrition Rates?](#), *Nat. Rev. Drug Discov.*, **3**: 711–716 (2004).
- [15] Prati F., Uliassi E., Bolognesi M.L., [Two Diseases, one Approach: Multitarget Drug Discovery in Alzheimer's and Neglected Tropical Diseases](#), *Medchemcomm*, **5**: 853–861 (2014).
- [16] Cavalli A., Bolognesi M.L., Minarini A., Rosini M., Tumiatti V., Recanatini M., Melchiorre C., [Multi-Target-Directed Ligands to Combat Neurodegenerative Diseases](#), *J. Med. Chem.*, **51**: 347–372 (2008).

- [17] Nepovimova E., Uliassi E., Korabecny J., Pena-Altamira L.E., Samez S., Pesaresi A., Garcia G.E., Bartolini M., Andrisano V., Bergamini C., [Multitarget drug Design Strategy: Quinone–Tacrine Hybrids Designed to Block Amyloid- \$\beta\$  Aggregation and to Exert Anticholinesterase and Antioxidant Effects](#), *J. Med. Chem.*, **57**: 8576–8589 (2014).
- [18] Nepovimova E., Korabecny J., Dolezal R., Babkova K., Ondrejicek A., Jun D., Sepsova V., Horova A., Hrabnova M., Soukup O., [Tacrine–Trolox Hybrids: A Novel Class of Centrally Active, Nonhepatotoxic Multi-Target-Directed Ligands Exerting Anticholinesterase and Antioxidant Activities with Low in Vivo Toxicity](#), *J. Med. Chem.*, **58**: 8985–9003 (2015).
- [19] Perez L.R., Franz K.J., [Minding Metals: Tailoring Multifunctional Chelating Agents for Neurodegenerative Disease](#), *Dalt. Trans.*, **39**: 2177–2187 (2010).
- [20] Scott L.E., Orvig C., [Medicinal Inorganic Chemistry Approaches to Passivation and Removal of Aberrant Metal Ions in Disease](#), *Chem. Rev.*, **109**: 4885–4910 (2009).
- [21] Ain Q., Batool M., Choi S., [TLR4-Targeting Therapeutics: Structural Basis and Computer-Aided Drug Discovery Approaches](#), *Molecules*, **25**: 627 (2020).
- [22] Batool M., Ahmad B., Choi S., [A Structure-Based Drug Discovery Paradigm](#), *Int. J. Mol. Sci.*, **20**: 2783 (2019).
- [23] Usha T., Shanmugarajan D., Goyal A.K., Kumar C.S., Middha S.K., [Recent Updates on Computer-Aided Drug Discovery: Time for a Paradigm Shift](#), *Curr. Top. Med. Chem.*, **17**: 3296–3307 (2017).
- [24] Viana J. de O., Félix M.B., Maia M. dos S., Serafim V. de L., Scotti L., Scotti M.T., [Drug Discovery and Computational Strategies in the Multitarget Drugs Era](#), *Brazilian J. Pharm. Sci.*, **54**: (2018).
- [25] Abdolmaleki A., Ghasemi J.B., Ghasemi F., [Computer Aided Drug Design for Multi-Target Drug Design: SAR/QSAR, Molecular Docking And Pharmacophore Methods](#), *Curr. Drug Targets.*, **18**: 556–575 (2017).
- [26] Carabet L.A., Rennie P.S., Cherkasov A., [Therapeutic Inhibition of Myc in Cancer. Structural Bases and Computer-aided Drug Discovery Approaches](#), *Int. J. Mol. Sci.*, **20**: 120 (2019).
- [27] Ganjali Koli M., Azizi K., [The Partition and Transport Behavior Of Cytotoxic Ionic Liquids \(ILs\) Through the DPPC Bilayer: Insights from Molecular Dynamics Simulation](#), *Mol. Membr. Biol.*, **33**: 64–75 (2017).
- [28] Koli M.G., Azizi K., [Investigation of Benzodiazepines \(BZDs\) in a DPPC Lipid Bilayer: Insights from Molecular Dynamics Simulation and DFT Calculations](#), *J. Mol. Graph. Model.*, **90**: 171–179 (2019).
- [29] Azizi M.G.K. K., [Molecular Dynamics Simulations of Oxprenolol and Propranolol in a DPPC Lipid Bilayer](#), *J. Mol. Graph. Model.*, **64**: 153–164 (2016).
- [30] Aghazadeh H., Ganjali Koli M., Ranjbar R., Pooshang Bagheri K., [Interactions of GF-17 Derived from LL-37 Antimicrobial Peptide with Bacterial Membranes: A Molecular Dynamics Simulation Study](#), *J. Comput. Aided. Mol. Des.*, **34**: 1261–1273 (2020).
- [31] Gobbo D., Cavalli A., Ballone P., Benedetto A., [Computational Analysis of the Effect of \[Tea\]\[Ms\] and \[Tea\]\[H 2 PO 4\] Ionic Liquids on the Structure and Stability of A \$\beta\$  \(17–42\) Amyloid Fibrils](#), *Phys. Chem. Chem. Phys.*, **23**: 6695–6709 (2021).
- [32] Yu W., MacKerell A.D., [Computer-Aided Drug Design Methods](#), In: *Antibiotics*, Springer, 85–106 (2017).
- [33] Eslami M., Hashemianzadeh S.M., Bagherzadeh K., Seyed Sajadi S.A., [Molecular Perception of Interactions between bis \(7\) Tacrine and Cystamine-Tacrine Dimer with Cholinesterases as the Promising Proposed Agents for the Treatment of Alzheimer’s Disease](#), *J. Biomol. Struct. Dyn.*, **34**: 855–869 (2016).
- [34] Eslami M., Hashemianzadeh S.M., Moghaddam K.G., Khorsandi-Lagol A., Sajadi S.A.S., [Computational Evidence to Design An Appropriate Candidate for the Treatment of Alzheimer’s Disease Through Replacement of the Heptamethylene Linker of Bis \(7\) Tacrine with S-Allylcysteine](#), *RSC Adv.*, **5**: 66840–66851 (2015).
- [35] Roosta S., Majid Hashemianzadeh S., Ganjali Koli M., [Investigation of Glutathione as a Natural Antioxidant and Multitarget Inhibitor for Alzheimer’s Disease: Insights from Molecular Simulations](#), *J. Mol. Liq.*, 117960 (2021).

- [36] Neumann U., Ufer M., Jacobson L.H., Rouzade-Dominguez M., Huledal G., Kolly C., Lüönd R.M., Machauer R., Veenstra S.J., Hurth K., [The BACE-1 inhibitor CNP 520 for prevention trials in Alzheimer's Disease](#), *EMBO Mol. Med.*, **10**: e9316 (2018).
- [37] Cheung J., Gary E.N., Shiomi K., Rosenberry T.L., [Structures of Human Acetylcholinesterase Bound to Dihydropyridone I and Teritrem B Show Peripheral Site Flexibility](#), *ACS Med. Chem. Lett.*, **4**: 1091–1096 (2013).
- [38] Davies M., Nowotka M., Papadatos G., Dedman N., Gaulton A., Atkinson F., Bellis L., Overington J.P., [ChEMBL web Services: Streamlining Access to Drug Discovery Data and Utilities](#), *Nucleic Acids Res.*, **43**: W612–W620 (2015).
- [39] Mendez D., Gaulton A., Bento A.P., Chambers J., De Veij M., Félix E., Magariños M.P., Mosquera J.F., Mutowo P., Nowotka M., [ChEMBL: Towards Direct Deposition of Bioassay Data](#), *Nucleic Acids Res.*, **47**: D930–D940 (2019).
- [40] Gilson M.K., Liu T., Baitaluk M., Nicola G., Hwang L., Chong J., [BindingDB in 2015: A Public Database for Medicinal Chemistry, Computational Chemistry and Systems Pharmacology](#), *Nucleic Acids Res.*, **44**: D1045–D1053 (2016).
- [41] Lo Monte F., Kramer T., Gu J., Anumala U.R., Marinelli L., La Pietra V., Novellino E., Franco B., Demedts D., Van Leuven F., [Identification of Glycogen Synthase Kinase-3 Inhibitors with a Selective Sting for Glycogen Synthase Kinase-3 \$\alpha\$](#) , *J. Med. Chem.*, **55**: 4407–4424 (2012).
- [42] Word J.M., Lovell S.C., Richardson J.S., Richardson D.C., [Asparagine and Glutamine: Using Hydrogen Atom Contacts in the Choice of Side-Chain Amide Orientation](#), *J. Mol. Biol.*, **285**: 1735–1747 (1999).
- [43] Morris G.M., Huey R., Lindstrom W., Sanner M.F., Belew R.K., Goodsell D.S., Olson A.J., [AutoDock4 and AutoDockTools4: Automated Docking with Selective Receptor Flexibility](#), *J. Comput. Chem.*, **30**: 2785–2791 (2009).
- [44] Berendsen H.J.C., van der Spoel D., van Drunen R., [GROMACS: A Message-Passing Parallel Molecular Dynamics Implementation](#), *Comput. Phys. Commun.*, **91**: 43–56 (1995).
- [45] Pall S., Abraham M.J., Kutzner C., Hess B., Lindahl E., ["Tackling Exascale Software Challenges in Molecular Dynamics Simulations with GROMACS"](#), in: *Int. Conf. Exascale Appl. Softw.*, Springer, pp. 3–27 (2014).
- [46] Abraham M.J., Murtola T., Schulz R., Páll S., Smith J.C., Hess B., Lindahl E., [GROMACS: High Performance Molecular Simulations Through Multi-Level Parallelism from Laptops to Supercomputers](#), *SoftwareX*, **1**: 19–25 (2015).
- [47] Vanommeslaeghe K., Hatcher E., Acharya C., Kundu S., Zhong S., Shim J., Darian E., Guvench O., Lopes P., Vorobyov I., [CHARMM General Force Field: A Force Field for Drug-Like Molecules Compatible with the CHARMM All-Atom Additive Biological Force Fields](#), *J. Comput. Chem.*, **31**: 671–690 (2010).
- [48] Bjelkmar P., Larsson P., Cuendet M.A., Hess B., Lindahl E., [Implementation of the CHARMM Force Field in GROMACS: Analysis of Protein Stability Effects from Correction Maps, Virtual Interaction Sites, and Water Models](#), *J. Chem. Theory Comput.*, **6**: 459–466 (2010).
- [49] Hoover W.G., [Constant-Pressure Equations of Motion](#), *Phys. Rev. A*, **34**: 2499 (1986).
- [50] Parrinello M., Rahman A., [Crystal Structure and Pair Potentials: A Molecular-Dynamics Study](#), *Phys. Rev. Lett.*, **45**: 1196 (1980).
- [51] Hess B., Bekker H., Berendsen H.J.C., Fraaije J.G.E.M., [LINCS: A Linear Constraint Solver for Molecular Simulations](#), *J. Comput. Chem.*, **18**: 1463–1472 (1997).
- [52] Hockney R.W., Goel S.P., Eastwood J.W., [Quiet High-Resolution Computer Models of a Plasma](#), *J. Comput. Phys.*, **14**: 148–158 (1974).
- [53] Darden T., York D., Pedersen L., [Particle Mesh Ewald: An  \$N \cdot \log\(N\)\$  Method for Ewald Sums in Large Systems](#), *J. Chem. Phys.*, **98**: 10089–10092 (1993).
- [54] Jorgensen W.L., Chandrasekhar J., Madura J.D., Impey R.W., Klein M.L., [Comparison of Simple Potential Functions for Simulating Liquid Water](#), *J. Chem. Phys.* **79**: 926–935 (1983).
- [55] Snyman J., [Practical Mathematical Optimization: An Introduction to Basic Optimization Theory and Classical and New Gradient-Based Algorithms](#), Springer Science & Business Media, (2005).

- [56] Humphrey W., Dalke A., Schulten K., [VMD: Visual Molecular Dynamics](#), *J. Mol. Graph.*, **14**: 33–38 (1996).
- [57] Kumari R., Kumar R., Consortium O.S.D.D., Lynn A., [g\\_mmpbsa-A GROMACS Tool for High-Throughput MM-PBSA Calculations](#), *J. Chem. Inf. Model.*, **54**: 1951–1962 (2014).
- [58] Srivastava A., Rawat P., Tandon P., Singh R.N., [A Computational Study on Conformational Geometries, Chemical Reactivity and Inhibitor Property of an Alkaloid Bicuculline with  \$\gamma\$ -aminobutyric Acid \(GABA\) by DFT](#), *Comput. Theor. Chem.*, **993**: 80–89 (2012).
- [59] Gohlke H., Kiel C., Case D.A., [Insights into Protein–Protein Binding by Binding Free Energy Calculation and Free Energy Decomposition for the Ras–Raf and Ras–RalGDS Complexes](#), *J. Mol. Biol.*, **330**: 891–913 (2003).
- [60] Zou B., Wang D.D., Ma L., Chen L., Yan H., [Analysis of the Relationship Between Lung Cancer Drug Response Level and Atom Connectivity Dynamics Based on Trimmed Delaunay Triangulation](#), *Chem. Phys. Lett.*, **652**: 117–122 (2016).
- [61] Zou B., Lee V.H.F., Chen L., Ma L., Wang D.D., Yan H., [Deciphering Mechanisms of Acquired T790M Mutation After EGFR Inhibitors for NSCLC by Computational Simulations](#), *Sci. Rep.*, **7**: 1–13 (2017).
- [62] Ducati R.G., Basso L.A., Santos D.S., de Azevedo Jr W.F., [Crystallographic and Docking Studies of Purine Nucleoside Phosphorylase from Mycobacterium Tuberculosis](#), *Bioorg. Med. Chem.*, **18**: 4769–4774 (2010).
- [63] Morrone Xavier M., Sehnem Heck G., Boff de Avila M., Maria Bernhardt Levin N., Oliveira Pintro V., Lemes Carvalho N., Filgueira de Azevedo W., [SAnDReS a Computational Tool for Statistical Analysis of Docking Results and Development of Scoring Functions](#), *Comb. Chem. High Throughput Screen.*, **19**: 801–812 (2016).
- [64] Wu J., Sun Y., Zhou H., Ma Y., Wang R., [Design, Synthesis, Biological Evaluation And Molecular Dynamics Simulation Studies of \(R\)-5-methylthiazolidin-4-One Derivatives as Megakaryocyte Protein Tyrosine Phosphatase 2 \(PTP-MEG2\) Inhibitors for the Treatment of Type 2 Diabetes](#), *J. Biomol. Struct. Dyn.*, **38**: 3156–3165 (2020).
- [65] Zhang L., Wang P., Yang Z., Du F., Li Z., Wu C., Fang A., Xu X., Zhou G., [Molecular Dynamics Simulation Exploration of the Interaction Between Curcumin and Myosin Combined with the Results of Spectroscopy Techniques](#), *Food Hydrocoll.*, **101**: 105455 (2020).
- [66] Amir M., Ahmad S., Ahamad S., Kumar V., Mohammad T., Dohare R., Alajmi M.F., Rehman T., Hussain A., Islam A., [Impact of Gln94Glu Mutation on the Structure And Function of Protection of Telomere 1, A Cause of Cutaneous Familial Melanoma](#), *J. Biomol. Struct. Dyn.* (2019).
- [67] Guinto Jr F.C., [Investigating Secondary Structure Features of YAP1 Protein Fragments Using Molecular Dynamics \(MD\) and Steered Molecular Dynamics \(SMD\) Simulations](#), PhD dissertation., University of the Pacific, (2017).
- [68] Soni S., Tyagi C., Grover A., Goswami S.K., [Molecular Modeling and Molecular Dynamics Simulations Based Structural Analysis of the SG2NA Protein Variants](#), *BMC Res. Notes.*, **7**: 1–16 (2014).
- [69] Laskowski R.A., MacArthur M.W., Moss D.S., Thornton J.M., [PROCHECK: A Program to Check the Stereochemical Quality of Protein Structures](#), *J. Appl. Crystallogr.*, **26**: 283–291 (1993).
- [70] Laskowski R.A., Rullmann J.A.C., MacArthur M.W., Kaptein R., Thornton J.M., [AQUA and PROCHECK-NMR: Programs for Checking the Quality of Protein Structures Solved by NMR](#), *J. Biomol. NMR.*, **8**: 477–486 (1996).